# Energetics and Partition of Two Cecropin-Melittin Hybrid Peptides to Model Membranes of Different Composition

Margarida Bastos,* Guangyue Bai,* Paula Gomes,* David Andreu,† Erik Goormaghtigh,‡ and Manuel Prieto§
*CIQ (UP) Department of Chemistry, Faculty of Sciences, University of Porto, P-4169-007 Porto, Portugal; †Proteomics & Protein Chemistry, DCEXS-UPF-PRBB, E-08003 Barcelona, Spain; ‡Structure and Function of Biological Membranes, Université Libre de Bruxelle, Brussels, Belgium; and §CQFM, Instituto Superior Técnico, UTL, P-1049-001 Lisbon, Portugal

ABSTRACT The energetics and partition of two hybrid peptides of cecropin A and melittin (CA(1–8)M(1–18) and CA(1–7)M(2–9)) with liposomes of different composition were studied by time-resolved fluorescence spectroscopy, isothermal titration calorimetry, and surface plasmon resonance. The study was carried out with large unilamellar vesicles of three different lipid compositions: 1,2-dimyristoil-*sn*-glycero-3-phosphocholine (DMPC), 1,2-dimyristoyl-*sn*-glycero-3-phospho-rac-(1-glycerol) (DMPG), and a 3:1 binary mixture of DMPC/DMPG in a wide range of peptide/lipid ratios. The results are compatible with a model involving a strong electrostatic surface interaction between the peptides and the negatively charged liposomes, giving rise to aggregation and precipitation. A correlation is observed in the calorimetric experiments between the observed events and charge neutralization for negatively charged and mixed membranes. In the case of zwitterionic membranes, a very interesting case study was obtained with the smaller peptide, CA(1–7)M(2–9). The calorimetric results obtained for this peptide in a large range of peptide/lipid ratios can be interpreted on the basis of an initial and progressive surface coverage until a threshold concentration, where the orientation changes from parallel to perpendicular to the membrane, followed by pore formation and eventually membrane disruption. The importance of negatively charged lipids on the discrimination between bacterial and eukaryotic membranes is emphasized.

## INTRODUCTION

The increasing prevalence of multiresistant microbial strains is driving extensive research for new type of antibiotics (1–5). Among these, antimicrobial peptides (AMP) have been widely studied in past years, as they may become an alternative to conventional antibiotic therapy (2,6–17). In fact, it has been claimed that cationic antimicrobial peptides exploit fundamental features of the bacterial cell so that resistance is much less likely to evolve than in the case of conventional antibiotics (7,18–20).

Over the years, efforts have been directed toward the increase in potency and specificity of AMPs against pathogenic agents while minimizing their cytotoxic effect toward eukaryotic cells. One particularly successful approach is based on hybrid sequences or chimera, derived from naturally occurring $\alpha$-helical AMPs cecropin A (CA) and melittin (M), which provided the first examples of AMP sequence hybridization (21,22). One such hybrid peptide, CA(1–8)M(1–18), showed improved antimicrobial activity relative to parent cecropin A and greatly reduced the hemolytic properties of melittin (23). Taking CA(1–8)M(1–18) as the lead, a subsequent approach was to further reduce the size of the hybrid CA-M peptides while retaining antimicrobial activity. This led to CA(1–7)M(2–9), a pentadecapeptide that preserves most of the activity of the parent lead peptide (24).

Their amino acid sequences are shown in Table 1, along with their helical wheel and $\beta$-sheet projections in Fig. 1. Both hybrids share the cationic N-terminus of cecropin A followed by the hydrophobic N-terminus of melittin, but CA(1–8)M(1–18) has a larger hydrophobic domain than CA(1–7)M(2–9).

Both CA(1–8)M(1–18) and CA(1–7)M(2–9) have been extensively studied in terms of antimicrobial activity (25–31), as well as on their membrane interaction properties (6,28–33). The characteristics of the peptide-membrane interaction process are dependent on the charge properties of the membrane and can be used to interpret the specificity of peptide activity against pathogens (12,18,29,34–39).

Following our previous study with these peptides, where their effect on vesicle thermotropic phase behavior, charge, and size could be related to membrane-induced changes in peptide structure (6), we have now addressed the energetics of the interactions as well as the partition of the peptides to the membranes and their relative position depending on peptide concentration.

Large unilamellar vesicles (LUVs) of three different lipid compositions were used: zwitterionic 1,2-dimyristoyl-*sn*-glicero-3-phosphocholine (DMPC), anionic 1,2-dimyristoyl-*sn*-glycero-3-[phospho-rac-(1-glycerol)] (DMPG), and a DMPC/DMPG (3:1) mixture. The study was carried out by time-resolved fluorescence spectroscopy (TRFS), isothermal titration calorimetry, and surface plasmon resonance (SPR).

*Submitted August 3, 2007, and accepted for publication October 23, 2007.*

Address reprint requests to Margarida Bastos, Fax: 351-22-0402659; E-mail: mbastos@fc.up.pt.

Editor: Petra Schwille.



0006-3495/08/03/2128/14 $2.00

doi: 10.1529/biophysj.107.119032

**TABLE 1 Sequences of cecropin A, melittin, and the hybrid peptides CA(1–7)M(2–9) and CA(1–8)M(1–18)**

| Peptide | Sequence |
|---|---|
| Cecropin A | H-KWKLFKKIEKVGQNIRDGIIKAGPAVAVVGQATQIAKK-$NH_2$ |
| Melittin | H-GIGAVLKVLTTGLPALISSWIKRKRQQ-$NH_2$ |
| CA(1–7)M(2–9) | H-KWKLFKKIGAVLKVL-$NH_2$ |
| CA(1–8)M(1–18) | H-KWKLFKKIGIGAVLKVLTTGLPALIS-$NH_2$ |

## MATERIALS AND METHODS

### Materials

DMPC and DMPG were obtained from Avanti Polar Lipids (Alabaster, AL) and used without further purification. Fmoc-protected amino acids, coupling reagents, and resins for solid-phase peptide synthesis were purchased from Bachem (Weil am Rhein, Germany). All other reagents were from Sigma Chemical (St. Louis, MO).

Peptide solutions and liposome suspensions were prepared in HEPES buffer (*N*-(2-hydroxyethyl) piperazine-*N′*-ethane-sulphonic acid). Ultra pure water (Milli Q Gradient, Millipore, Billerica, MA) was used in the preparation of all samples.

### Vesicle preparation

Appropriate amounts of phospholipids (DMPC, DMPG, and DMPC/DMPG (3:1)) were dissolved in chloroform (DMPC) or chloroform/methanol (3:1 v/v) (DMPG and DMPC/DMPG (3:1)). The samples were then dried under a nitrogen stream, and the film was kept under vacuum for 3 h to remove all traces of organic solvents. The resulting lipid film was warmed together with HEPES buffer (10 mM Hepes, 100 mM NaCl, pH 7.4) in a thermostated water bath at ~10°C above the temperature of the gel-to-liquid crystalline phase transition ($T_m$), and then hydrated at the same temperature. The multilamellar vesicles thus obtained were frozen in liquid nitrogen and thawed in a water bath at ~10°C above $T_m$, and this process was repeated five times.

Large unilamellar vesicles (LUVs) were obtained from the multilamellar vesicles by extrusion in a 10 mL stainless steel extruder (Lipex Biomembranes, Vancouver, British Columbia, Canada), thermostated with a recirculating water bath, at ~10°C above $T_m$. The samples were passed several times through polycarbonate filters (Nucleopore, Pleasanton, CA) of decreasing pore size (600, 200, and 100 nm—5, 5, and 10 times, respectively), under inert ($N_2$) atmosphere.

Size distribution of extruded vesicles was determined by dynamic light scattering (Zetasizer nanoZS, Malvern Instruments, Malvern, Worcestershire, UK) at 37°C, using a He-Ne laser (wavelength 633 nm) as a source of incident light, and operating at a scattering angle of 173°. Mean particle size was thus determined as being of (106 ± 4) nm (average and standard deviation of six independent measurements). The phospholipid concentration was determined by the phosphomolibdate method (40).

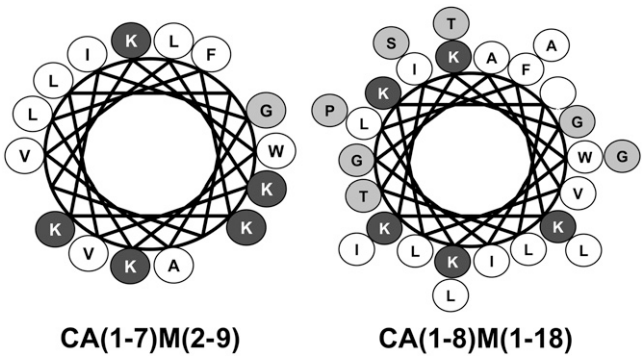


FIGURE 1 Helical wheel representation of CA(1–7)M(2–9) and CA(1–8)M(1–18): light gray, polar, noncharged residues; dark gray, polar, positively charged residues; and white, hydrophobic residues.

### Peptides synthesis and solution

The studied peptides, CA(1–7)M(2–9) and CA(1–8)M(1–18), were synthesized as C-terminal carboxamides by Fmoc/tBu solid phase strategies, purified, and characterized by methods as those described in Gomes et al. (41). Peptide stock solutions were prepared in HEPES buffer (10 mM; 0.1 M NaCl; pH 7.4) in the 2–5 mM concentration range, and quantitated by either amino acid analysis (AAA) or ultraviolet absorption at 280 nm, taking 5690 $M^{-1}.cm^{-1}$ as the molar extinction coefficient corresponding to the single tryptophan residue present in both studied peptides (42).

### Time-resolved fluorescence spectroscopy

Stock solutions (6 mM) of LUVs of the three membrane systems (DMPC, DMPG, and DMPC/DMPG) were prepared in the buffer as above. Unless otherwise stated, the concentration of the peptide solutions in the same buffer was 20 $\mu$M. Addition of appropriate volumes of liposome suspension into the peptide solution was performed so as to cover a range of liposome concentrations (0–6 mM). Measurements were performed for the pure peptide solution and at increasing liposome concentration. The mixtures were prepared (six independent mixtures for each peptide/membrane system) and allowed to equilibrate at 35°C for ~1/2 h before measurements. All measurements were performed at 35°C.

Fluorescence decay measurements were carried out with a single-photon timing system, which is described elsewhere (43). Sample was excited at 295 nm using a frequency doubled, cavity dumped (3.7 MHz repetition rate), dye laser of rhodamine 6G (Coherent (Santa Clara, CA) 701-2), synchronously pumped by a mode-locked $Ar^+$ laser (514.5 nm, Coherent Innova 400-10). The emission (at 316 nm) was detected by a Hamamatsu (Bridgewater, NJ) R-2809 MCP photomultiplier at 345 nm (Jobin-Yvon (Edison, NJ) HR320 monochromator). Timescales were chosen for each sample to observe the decay through 2–3 intensity decades. Experimental response functions for deconvolution were generated from a scattering dispersion (silica, colloidal water suspension, Aldrich, Milwaukee, WI). Data analysis was carried out using a nonlinear least squares iterative convolution method based on the Marquardt algorithm. The goodness of the fits was judged from the experimental $\chi^2$ values, weighted residuals, and autocorrelation plots.

The complex decay of tryptophan was described by a sum of exponentials,

$$I(t) = \sum_{i=1}^{n} \alpha_i e^{-t/\tau_i}, \quad (1)$$

where $\alpha_i$ and $\tau_i$ are the normalized amplitude ($\sum_i \alpha_i = 1$) and lifetime of the *i*th decay component, respectively.

From the fluorescence intensity decay kinetics of Trp residues, the amplitude-weighted mean fluorescence lifetime, $\bar{\tau}$, (also called the lifetime weighted quantum) was calculated as

$$\bar{\tau} = \sum_{i=1}^{n} \alpha_i \tau_i. \quad (2)$$

## Determination of partition constants

The association of the peptides to the model membranes can be described quantitatively as a first approximation in terms of a simple partition equilibrium between the aqueous and the lipid bilayer phase for amphipathic peptides, $P$,

$$K_{P,x} = \frac{\dfrac{n_L^P}{n_l + n_L^P}}{\dfrac{n_W^P}{n_w + n_W^P}}, \quad (3)$$

where $K_{P,x}$ represents the mole-fraction partition coefficient of the peptide, $n_W$ and $n_L$ are the amount (in mole) of water and lipid in each sample, and $n_i^P$ is the amount of peptide present in each phase ($i = W$, aqueous phase, and $i = L$, lipid phase, respectively). In all partitioning experiments, it is reasonable to assume that $n_W \gg n_W^P$, and because high membrane-bound concentrations of the peptide are usually avoided to prevent deviations from ideal partitioning due to peptide/peptide interactions at the water/membrane surface or in the lipid bilayer, it can also be considered that $n_L \gg n_L^P$. In these circumstances, Eq. 3 can be simplified:

$$K_{P,x} = \frac{\dfrac{n_L^P}{n_l}}{\dfrac{n_W^P}{n_w}}. \quad (4)$$

If the amounts of lipid and water ($n_W$ and $n_L$, respectively) are replaced by their respective volumes, a partition constant ($K_P$) related to the previous one is obtained, being

$$K_P = K_{P,x}\frac{\gamma_W}{\gamma_L}, \quad (5)$$

where $\gamma_w$ and $\gamma_L$ are the molar volumes of water and lipid. This second form of the partition constant was used.

The changes undergone by the peptides' fluorescence properties can be used to distinguish between free and membrane-bound peptide populations by time-resolved fluorescence measurements (fluorescence decays), and therefore can be applied to quantitatively evaluate its interaction with the lipid bilayers. Therefore, by use of the equations above, an equation relating the lifetime-weighted quantum yield, $\bar{\tau}$, to the partition coefficient can be derived:

$$\bar{\tau} = \frac{\bar{\tau}_W + K_P \times \gamma_L \times [L] \times \bar{\tau}_L}{1 + K_P \times \gamma_L \times [L]}. \quad (6)$$

This equation was fitted to the experimentally obtained data to get the partition coefficient of the peptide to the membrane, $K_P$, and the lifetime-weighted quantum yield in the membrane phase, $\bar{\tau}_L$. Although fluorescence steady-state data could be used for this purpose, in the strongly scattering solutions used, no reasonable fittings would be obtained. The integration of the decay, which is proportional to the quantum yield, is a much more reliable experimental approach. The lipid concentration was based on the outer-leaflet content (50% of total lipid content).

## Isothermal titration calorimetry

The calorimetric technique used was stepwise isothermal titration microcalorimetry. The water bath and peripheral units were built at Lund University, Lund, Sweden, and a twin heat conduction calorimeter (ThermoMetric, Järfälla, Sweden) was used with a 1 mL titration cell equipped with a gold stirrer. The instrument was calibrated electrically, using an insertion heater. The detailed calorimetric setup and basic procedure have been described previously (44). Briefly, in each titration, 0.9848 ± 0.0008 mL of sample (either liposome suspension or peptide solution) were placed in the titration cell and sequences of successive injections were made at 4 min intervals (injections with 20 min intervals did not reveal the presence of slow reactions). The temperature of the measurements was 35°C throughout, so that the recorded values refer to the interaction of the peptides with the liposomes in the fluid phase (6). Experiments were performed in the ''fast titration mode'', the resulting curves deconvoluted (45) and the integrals were calculated in V.s, and transformed to heat exchanged by the appropriate calibration constant. The obtained heats were corrected for the dilution effects as determined in separate experiments (they were only significant in the case of the titration of highly concentrated peptide solution into buffer).

Different experimental setups were used, regarding the relative positions of the peptides and the vesicles:

1. Very low peptide/lipid (P/L) ratios (~1:1500 or 1:3000)—injections of 12.46 μL peptide solution (1.7 mM for CA(1–7)M(2–9) and 0.72 mM for CA(1–8)M(1–18)) into liposome suspension in the cell (35 mM).
2. Intermediate P/L ratios (P/L from 1:333 to 1:14)—injections of 2.66 μL peptide solution (5.38 mM) into liposome suspension in the cell (5.85 mM). This setup was only used for CA(1–7)M(2–9) with DMPC (see below).
3. Very high P/L ratios (1:2–1:33)—injections of 2.66 μL liposome suspension (35 mM) into peptide solution in the cell (20–50 μM).

## Surface plasmon resonance

SPR analyses were run on a Biacore 3000 (Biacore, Uppsala, Sweden) using L1 sensor chips (Biacore) for vesicle (LUVs) capture and subsequent formation of the lipid bilayer (46,47). Phosphate-buffered saline (PBS,100 mM at pH 6.81) was used as running buffer and to prepare the peptide solutions as well. Other buffers (e.g., HEPES) were tested, but led to higher baseline drifts. All peptide solutions were freshly prepared, buffer degassed, and filtered through a 0.22 μM filter. Before liposome immobilization and interaction analysis, the L1 sensor chips were rinsed with running buffer and then washed with a 25-μL injection of 40 mM *N*-octyl-β,D-glucopyranoside (OG) at a flow rate of 5 μL/min. LUVs (1 mM in PBS) were then injected (30 μL) at a 2 μL/min flow rate, after which the surface was rinsed with 50 μL of 10 mM NaOH at a flow rate of 50 μL/min to remove any multilamellar structures from the lipid surface (46,47). This procedure reproducibly led to the desired lipid bilayers with stable baseline signals. Peptide-lipid binding assays were performed through sequential injections of peptide solutions in PBS at four different concentrations, ranging from 12.5 to 100 μM, using a 10 μL/min buffer flow rate to avoid mass-transport limitations. Once the injection had ended, the buffer flow was continued to allow for a dissociation period of 450 s. As the initial baseline level was not recovered after this dissociation step, and not even after washing the surface with NaOH (50 μL) and HCl (50 μL) at 50 μL/min, the lipid bilayer was stripped out with a 30-μL injection of OG (at 5 μL/min) after each peptide injection and the liposome immobilization was repeated before the subsequent injection. The sensorgrams obtained for each peptide-lipid interaction were tentatively processed by curve fitting with numerical integration analysis, using the BIA evaluation 3.0.1 software. This study was done at 25°C and 35°C, and all analyses were run in duplicate.

# RESULTS AND DISCUSSION

## Partition constants and life-time weighted quantum yields

The results obtained for both peptides and the three lipid systems are plotted in Fig. 2, *A* and *B*, for CA(1–7)M(2–9) and CA(1–8)M(1–18), respectively. Equation 6 was fitted to the experimental results, representing a model that considers a simple partition for the peptide between the aqueous media and the membrane. Some peculiarities were observed for both peptides.

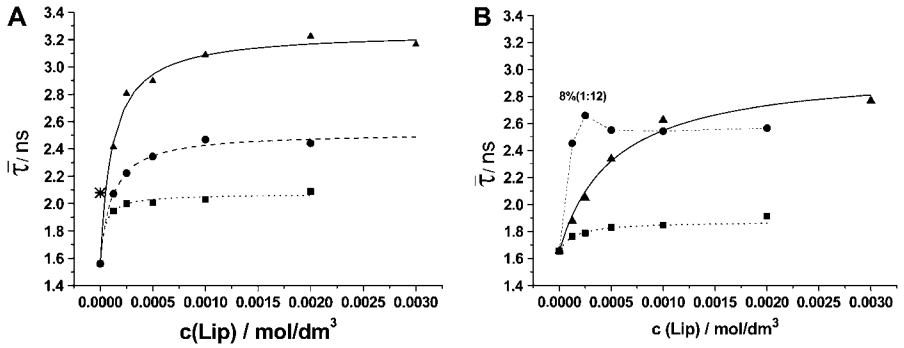


FIGURE 2 Plot of the obtained values of $\bar{\tau}$, the amplitude-weighted mean fluorescence lifetime (Eq. 2), as a function of lipid concentration (outer leaflet, see text), for the three studied systems, at 35°C. The symbols represent the experimental values, and the lines are the fitted curves according to Eq. 6. (*Symbols*) (▲) DMPC, (●) DMPC/DMPG (3:1), and (■) DMPG. (*) represents the experimental value for $\bar{\tau}_w$ for CA(1–8)M(1–18) at concentration of 20 $\mu$M. The open symbol was obtained from model fitting (see text for details). (*Lines*) DMPC (*solid*), DMPC/DMPG (3:1) (*dashed*), and DMPG (*dotted*). (*A*) CA(1–8)M(1–18); (*B*) CA(1-7)M(2–9) Note that in *B*, the broken line is not a fitted line, it just connects the experimental points. The values represented close to the experimental points are the peptide percent (based on the lipid content of the outer layer (see text)).

In the case of CA(1–7)M(2–9), the results with DMPC and DMPG are compatible with such a model under the conditions used, as can be seen in Fig. 2 *B*, where the obtained fitted lines are represented along with the experimental data. The fittings were performed with the lipid content based on the outer leaflet, i.e., half of the total lipid content. The obtained $K_p$ values were $(2.9 \pm 0.6) \times 10^3$ and $(10.6 \pm 1.5) \times 10^3$ and the corresponding values of the lifetime-weighted quantum yield in the membrane phase, $\bar{\tau}_L$, were (3.01 ± 0.09) and (1.87 ± 0.01) ns for DMPC and DMPG, respectively. For the mixed system, on the other hand, it was impossible to fit a curve reflecting a simple partition to the observed results—a very strong partition is observed until ~8% (peptide mol percentage) (based on the outer leaflet), and after that the lifetime-weighted quantum yield decreases. In Fig. 2 *B*, the obtained results for this system are connected by a broken line. If a fitting is performed by using just the first three values to get an insight into the magnitude of the partition in the initial part (high P/L ratios), a $K_p$ value of $1.0 \times 10^5$ is obtained. This value indicates a very strong partition to the mixed membrane at the initial stage of the fluorescence experiments. A curve was simulated using the first (value in buffer) and last points for comparative purposes, and the best parameters were $K_p = 1.3 \times 10^4$ and $\bar{\tau}_L = 2.6$. These values are both intermediate to the respective values found for the pure DMPC and pure DMPG systems.

For CA(1–8)M(1–18), the most remarkable feature was that in most cases the observed value for the lifetime-weighed quantum yield in buffer was higher than the corresponding values obtained in the presence of the membranes (Fig. 2 *A*). As we had previous knowledge that this peptide adopts a $\beta$-sheet structure—probably antiparallel—in buffer (6), we suspected that this indicates a strong association leading to a shielding of the Trp from the aqueous environment, even at the low peptide concentrations initially used (20 $\mu$M). The results from anisotropies also confirm a strong association (results not shown). Measurements of the peptide in buffer were performed at progressively lower peptide concentrations, leading to decreasing values of lifetime-weighed quantum yield, until a value of 1.86 ns was obtained at 3 $\mu$M (this was the lower limit that could be determined). Therefore, calculations were performed also allowing the lifetime-weighed quantum yield in buffer to be obtained as a fitting parameter, leading to a value of $\tau_w$ of 1.56 ns. This value was then used as a fixed parameter in all three fittings, producing $K_p$ values of $(36.1 \pm 9.8) \times 10^3$, $(13.3 \pm 1.6) \times 10^3$, and $(13.9 \pm 1.7) \times 10^3$, and $\bar{\tau}_L$ values of (2.07 ± 0.02), (3.26 ± 0.04), and (2.52 ± 0.03) ns for DMPG, DMPC, and DMPC/DMPG (3:1), respectively.

These results are summarized in Table 2, along with the enthalpies obtained from calorimetry and the thermodynamic parameters $\Delta G$ and $T\Delta S$ derived thereafter (see below).

## Energetics of the interaction

Type 1 experiments (very low P/L ratios, see above), where small aliquots of peptide solution were titrated into concentrated liposome suspensions, produced a constant heat release

**TABLE 2 Thermodynamic parameters for the interaction of the two peptides with the different membrane systems at 308.15 K, as obtained from calorimetry and TRFS**

| | | $\Delta H$/(kJ/mol) | $K_p^*$ | $\Delta G$/(kJ/mol) | T$\Delta S$/(kJ/mol) | $\tau_L$/ns* |
|---|---|---|---|---|---|---|
| DMPG | CA(1–7)M(2–9) | −46 ± 4 | $(1.06 \pm 0.15) \times 10^4$ | −33.1 | −12.9 | 1.87 ± 0.01 |
| | CA(1–8)M(1–18) | −43 ± 4 | $(3.61 \pm 0.98) \times 10^4$ | −36.3 | −6.7 | 2.07 ± 0.02 |
| DMPC | CA(1–7)M(2–9) | – | $(2.90 \pm 0.5) \times 10^3$ | −29.8 | – | 3.01 ± 0.09 |
| | CA(1–8)M(1–18) | −15 ± 2 | $(1.33 \pm 0.16) \times 10^4$ | −33.7 | 18.7 | 3.26 ± 0.04 |
| DMPG/DMPC | CA(1–7)M(2–9) | – | – | – | – | |
| | CA(1–8)M(1–18) | – | $(1.39 \pm 0.17) \times 10^4$ | –33.8 | – | 2.52 ± 0.03 |

*From TRFS.

per injection when DMPG was involved, indicating that at these low ratios the partition of both peptides to the negatively charged membrane is almost complete. To calculate the correct value for the respective enthalpies of interaction, the obtained results were nevertheless corrected by use of the partition coefficients obtained from TRFS $K_p$, (see below). The peptide partition to the negatively charged membrane under these conditions was 99.6% and 99.9% for CA(1–7)M(2–9) and CA(1–8)M(1–18), respectively. The obtained enthalpy values were ($-46 \pm 4$) and ($-43 \pm 4$) kJ/mol$_{(\text{peptide in the membrane})}$ for CA(1–7)M(2–9) and CA(1–8)M(1–18), respectively. The estimated precision of the enthalpy values was >10%, thus the enthalpy of interaction of both peptides with DMPG is the same, within experimental uncertainty.

Our partition coefficient can be easily transformed into the mole fraction partition coefficient (see Eq. 5 above), as $K_{p,x} = K_p \times (\gamma_L/\gamma_W)$, using the values 0.698 and 0.018 L/mol for the molar volumes of lipid and water (48), respectively, and the Gibbs energy change and entropy change can therefore be calculated as $\Delta G = -RT \ln(K_{p,x} \times 38.8)$ and $T\Delta S = \Delta H - \Delta G$. The Gibbs energy values so obtained were −33.1 and −36.3 kJ/mol, and the entropies, $T\Delta S$ −12.9 and −6.7 kJ/mol, for CA(1–7)M(2–9) and CA(1–8)M(1–18), respectively (Table 2).

Although with the pure negatively charged system the most important factor underlying the interaction is electrostatics, and both peptides have the same charge, this similarity in enthalpy and Gibbs energy changes for two peptides that are significantly different in length must also reflect that a different number of amino acids participates in the helical structure formed upon interaction with the membrane. It is known that the energetics of the transition from a random coil in solution to an $\alpha$-helix or a $\beta$-sheet in the membrane is consistent with the hypothesis that secondary structure formation at the membrane is driven by a reduction in the Gibbs energy of partition due to hydrogen bonding among the peptide amide groups (49,50). Furthermore, apparently it does not depend much either on the peptide or on the secondary structure type—Ladokhin and White found the $\Delta G_{residue}$ for melittin $\alpha$-helix formation at the POPC membrane interface to be similar to the value observed for $\beta$-sheet formation by $AcWL_5COO^-$, thus suggesting the value of $\Delta G_{residue} \approx -2$ kJ/mol$_{res}$ for estimating the energetic consequences of secondary structure on membranes (50). We can therefore compare our thermodynamic parameters with available data for other peptides. Although in most studies mixed membranes are used, there are some reports with pure negatively charged liposomes, such as the study by Ladokhin and White of the partition of native melittin and its diasteroisomer $D_4$,L-melittin (50). Wieprecht et al. (51) studied the energetics and partition of magainin-2-amide to LUVs of POPC/POPG (3:1) at 30°C and suggested the contribution of helix formation to the enthalpy of binding to be −3.3 kJ per mol of residues in the helix, and a contribution of helix formation to the total Gibbs energy of −0.5 kJ/mol$_{res}$. Even though we have a purely negative membrane, the energetics at very low P/L ratios are dominated by electrostatics, i.e., by the interaction with the negative parts of the membrane, as we will show later in this discussion. Therefore, we can use their equation to predict the contribution of the enthalpy of helix formation to the total enthalpy for each of our peptides. Bargava and Feix (32) reported results for the partition of CA(1–7)M(2–9) to LUVs of POPE/POPG (80:20) and POPE/POPG/CL (68:26:6) membranes, also at high ionic strength (20 mM MOPS and 100 mM KCl, pH 7.0), and low P/L ratios. Their results were compatible with the formation of a single $\alpha$-helix that encompasses the full length of the peptide, although the evidence for helical structure in the N-terminal half was less rigorous. Circular dichroism measurements showed that this peptide has a random structure in buffer, and no significant difference in the curves was found for this membrane system (DMPG) when the peptide content varied from 3 to 8 mol%, indicating a 78% helicity in these conditions (M. Bastos, unpublished data). Therefore, the initial estimate by Bargava and Feix (32) was probably too high—in fact, they recently reported (33) a smaller value (58%) in LUVs of POPE/POPG/CL (70:25:5) in 50 mM MOPS, pH 6.8 (unadjusted ionic strength). Taking our own estimation of 78%, the calculated value is −38 kJ/mol ($15 \times 0.78 \times (-3.3)$). This calculated value for the contribution of helix formation to the observed enthalpy thus represents 85% of our experimental value. This is very similar to the value of ~90% found by Wieprecht et al. for the partition of PGLa to POPC/POPG (3:1) membranes at 30°C, and the difference even goes along with a reduction in helix content as the temperature increases (our values are at 35°C, and they found that this contribution decreases to 68% at 45°C) (52).

As regarding CA(1–8)M(1–18), we can estimate a helix content for our DMPG system of ~40%, and we found this peptide to have a significant $\beta$-sheet structure in buffer (6). Ladokhin and White (50) also observed that melittin does not form a helix encompassing all residues in negatively charged membranes—they found a mean helical content of 71% when melittin partitions to LUVs of POPG, a value that is higher than our estimate for CA(1–8)M(1–18). The contribution of helix formation to the measured enthalpy would then amount to −34 kJ/mol ($26 \times 0.4 \times (-3.3)$) for this peptide, representing 80% of the measured enthalpy. This value is similar to the one found for the smaller peptide. We should stress, though, that in this case, the enthalpy change must also reflect partly the change from a partial $\beta$-sheet structure in buffer to an $\alpha$-helix at the membrane surface. Indeed, this amounts to saying that the measured enthalpies for peptide partition to a DMPG membrane mainly reflect the formation of an $\alpha$-helix at the negatively charged surface.

When the peptides were titrated into concentrated DMPC solutions under the same conditions (very low P/L ratios), two different situations occurred: i), in the case of CA(1–8)

M(1–18), a constant heat release was also observed, from which the interaction enthalpy was calculated, using again the partition coefficient obtained from TRFS (see above) to calculate the amount of peptide that partitions to the membrane (99.6%)—the value so obtained was (−15 ± 2) kJ/$mol_{(peptide\ in\ the\ membrane)}$; and ii), with CA(1–7)M(2–9), it was never possible to get a constant heat release, no matter how we changed and reduced the peptide concentration (within instrument sensitivity). The observations with CA(1–7)M(2–9) led us to use another set of P/L ratios (type 2 experiments), where a solution of peptide 5.85 mM ($v$ = 12.46 $\mu$L) was titrated into a DMPC suspension of concentration 5.85 mM, so as to fully investigate the behavior of this peptide with zwitterionic membranes in a very large P/L range. The obtained raw data for the type 2 setups can be seen in Fig. 3, *A–C*. Fig. 3 *A* shows the calorimetric raw data for the titration of a 1.7 mM peptide solution into a 31.85 mM DMPC suspension. We can see that the first five injections give rise to a positive effect: at the fifth injection, a negative contribution starts to appear (P/L = 1:270), the net heat exchange is zero at the eighth injection (P/L = 1:170), and from ninth injection through the end of the titration run a negative heat effect is recorded (P/L from 1:150 to 1:90). In Fig. 3 *B*, we show a plot of the calorimetric tracing for the second set of experimental conditions, with an enlargement of the first six injections presented in Fig. 3 *C*. In this last one, we can see that the first injection gives rise to an endothermic peak: from second (P/L = 1:184) to fifth (P:L = 1:74) injections, there is first a fast exothermic process that is followed by an endothermic one, and as the titration proceeds, the endothermic contribution decreases and the exothermic one increases, until eventually the endothermic contribution disappears from injection 6 (P/L = 1:61) to the end of the titration.

The integrated results were corrected for peptide dilution into buffer (small endothermic effect), as titration of buffer into the liposome suspension did not give rise to a significant heat effect. In Fig. 4, the corrected heats are plotted as a function of peptide % (100*$mol_{peptide}$/$mol_{lipid}$) for both types of experiments—titration into 35 mM DMPC (usual setup) and the type 2 setup just described above. In both cases, we can see that there is a heat release throughout the titration, but the curve growth depends on the P/L. Please note that the different slopes of the descending parts from both the titration setups reflect a different increase in the P/L ratio per injection. In both cases, the first injection(s) gave rise to a small, endothermic effect that turns negative at ~0.55% (peptide percentage) or 1:180 (P/L ratio). In the curve with intermediate P/L ratios (setup 2 above), and always referring to a total lipid content, we can see that there is an increasingly larger heat release per injection until a P/L ratio of 1:40; then a plateau region is observed until ~1:28, and thereafter the heat release is decreasingly negative. If we consider the injections that only give rise to a positive heat effect (first four injections when we titrate a 1.7 mM peptide solution into a 35 mM liposome suspension and the first injection for the

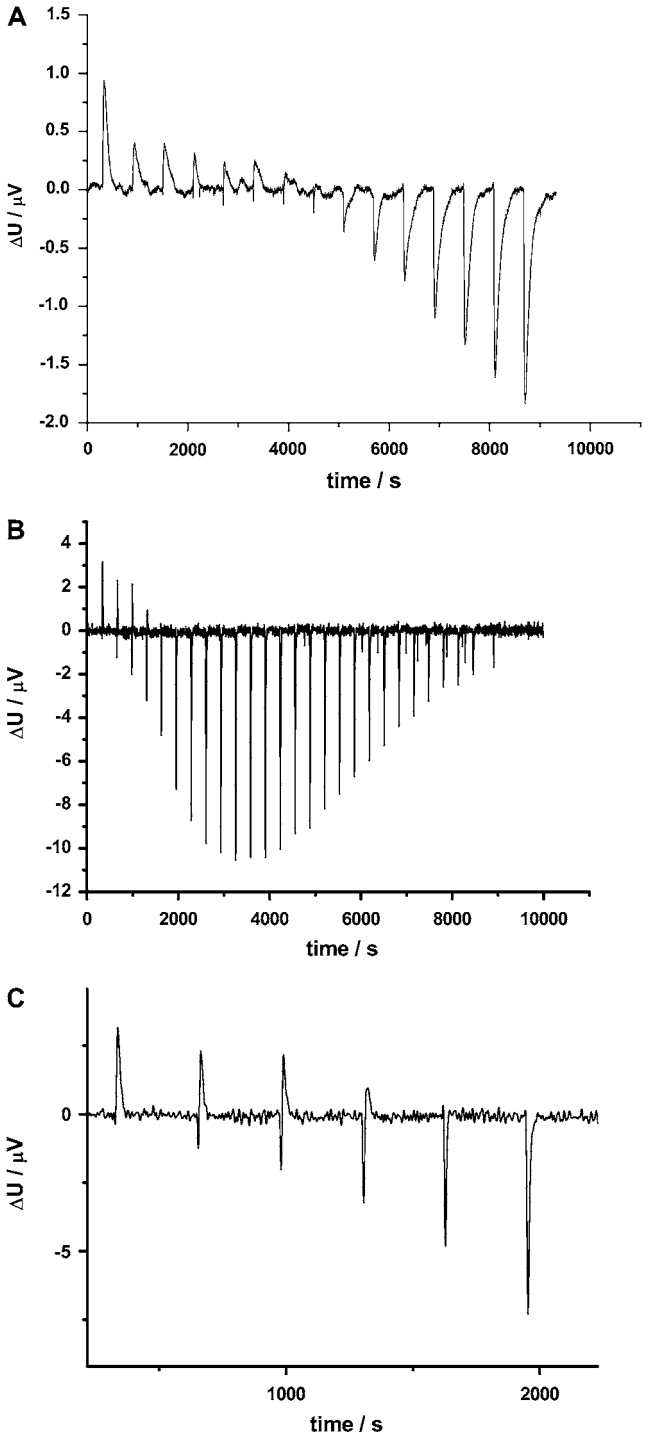


FIGURE 3 (*A*) Raw data (potential difference across the thermopiles as a function of time) for the titration of CA(1–7)M(2–9) ($c$ = 1.7 mmol/$dm^3$) into DMPC suspension in the vessel ($c$ = 31.85 mmol/$dm^3$). The injected volume was 12.46 $\mu$L per injection. (*B*) Raw data (potential difference across the thermopiles as a function of time) for the titration of CA(1–7)M(2–9) ($c$ = 5.38 mmol/$dm^3$) into DMPC suspension in the vessel ($c$ = 5.85 mmol/$dm^3$). The injected volume was 2.66 $\mu$L per injection. (*C*) Enlargement of the first six injections of the previous titration curve.

titration of 5.38 mM peptide into 5.85 mM liposome suspension), the enthalpy obtained either from the average of the first four injections or the single injection in the second case both produce a positive enthalpy value of +5 kJ/mol, corresponding in both cases to a maximum of 0.3% peptide. This heat pattern leads us to propose that this value can be tentatively assigned to the partition of CA(1–7)M(2–9) to the zwitterionic membrane without conformational transition to an $\alpha$-helix—that is, it represents the partition of the random coil from bulk solution to the membrane surface.

As can be inferred from what is described above, the partition profile of CA(1–7)M(2–9) to DMPC represents a very interesting case study, worthy of further discussion. Turning our attention to Fig. 3 (*squares* and *solid line*), we see that after crossing zero at ~0.6% (peptide molar percentage) (1:180), there is an increasingly negative heat response as the peptide content increases, until 2.5% (1:40). Analyzing the descendant and ascendant parts of the titration curve, we observe that whereas the heat release per injection is not constant within each part, its derivative is—the average increment on the descending part (until 2.5% (1:40)) is $-0.13 \pm 0.06$ mJ and on the ascending part it amounts to $(+0.05 \pm 0.02)$ mJ. On the descending part, this must be the reflection of a cooperative uptake. If we divide the decrement observed in the descendent part by the increase in peptide number of moles, we will get the value −9.2 kJ/mol. This is a reasonable value as compared to that of −15 kJ/mol obtained for the partition of CA(1–8)M(1–18) to DMPC. Nevertheless, it reflects a different behavior, as here it represents the increase in enthalpy per mole of peptide. Again, this cooperative behavior is in line with similar observations for this peptide already referred to above (32,33). Fernández et al. (53) have also found evidence for association of CA(1–7)M(2–9) in helix-inducing solvents, and suggested that aggregation of the helical peptide in membranes could result in an increase in its effective partition. Our plateau value occurs between 2.5% (1:40) and 3.5% (1:30), in remarkable agreement with the range where Pistolesi et al. (33) also found a plateau. Their sharp decrease at 1:25 is also almost the same value as ours, where the observed heat release starts to decrease.

If we consider the initial study of Bhargava and Feix for very low peptide content (32), we can assume that we also have CA(1–7)M(2–9) in the beginning of the titration as an $\alpha$-helix parallel to the membrane surface. Our FTIR results (not shown), on the other hand, indicate that already at 1%, there is a transmembrane helix. Nevertheless, we should stress that in the FTIR measurements, we have only a lipid monolayer with minimal hydration, and thus the results can differ from what is observed in liposome suspensions, as it has been already referred that melittin orientation in a membrane depends critically on the hydration level. This shows that our peptide can change from parallel to perpendicular to the membrane surface already at low peptide content. It has been reported that CA(1–7)M(2–9) is not long enough to span the whole length of the bilayer when in helical form (54), as the length of the $\alpha$-helix of a 15-residue analog is ~22.5 Å. This can be the reason for the cooperative uptake—the need for two helices to span the lipid bilayer can promote a higher peptide partition. After 3.5%, the heat release starts to decrease. As pore formation is known to be an endothermic process, we propose that this decrease reflects pore formation. In this line of reasoning, the plateau value can be tentatively interpreted as reflecting a range of P/L ratios where we are close to membrane saturation and there is a balance between peptide partition and pore formation.

After the threshold value of 3.5%, pore formation increases at every rise in peptide content. A maximum in the dichroic ratio for the peptide amide I was also observed in the FTIR measurements for 3% peptide, with a decrease thereafter to close to the initial values. It was further noted that at all studied peptide contents (from 1 to 10%), the value for the dichroic ratio for the lipid carbonyl was rather constant, and the lipid showed a remarkable order in the presence of growing amounts of peptide (M. Bastos and E. Goormaghtigh, unpublished results). This observation is in line with what was found by Pistolesi et al. (33), where they point out that, as the peptide concentration increased, the lipid systems reverted to a behavior similar to that observed in the absence of peptide. They interpret their results as possibly meaning that, after a threshold concentration, the peptide becomes sequestered (i.e., in localized pores), leaving the bulk lipid phase rather unperturbed.

We agree with this view, and extend it further as we believe that this segregation occurs early (indicated by a very high and constant lipid ordering as suggested by FTIR), and is responsible for the cooperative uptake. Probably in this pure zwitterionic membrane, only transient toroidal pores are first observed, whereas after 3% more permanent ones are formed. One could also think of membrane solubilization as the final stage of membrane disruption. Nevertheless, this contradicts the return to unperturbed behavior observed by Pistolesi et al. (33) and ourselves by FTIR. So we tend to find more realistic the first explanation as it encompasses all known results.

Now looking at the ascendant part of the titration curve, we find that again only the derivative of the heat as a function of concentration is constant, namely at $(+0.05 \pm 0.02)$ mJ. Dividing this value by the increase in the number of moles of peptide per injection, we get the value of +3.5 kJ/mol. We would tentatively assign this value to the enthalpy of pore formation for this system. This value is smaller than the one proposed by Wenk and Seelig (55), namely $(+26 \pm 4)$ kJ/mol for magainin interaction with POPC/POPG membranes. Nevertheless, we should remember that their membrane systems are partly negatively charged, so the difference is not surprising. To the best of our knowledge, our value is the second value provided in the literature for the enthalpy of pore formation by antimicrobial peptides.

When setup 3 was used, i.e., titration of liposome suspension into peptide solution (see Materials and Methods), the results depended again strongly on the lipid system.

For DMPC, no resolvable peaks were obtainable within the instrument sensitivity. With the purely negatively charged system (DMPG), an exothermic process was always observed. Nevertheless, no binding curve was obtained. Considering that each peptide has a +5.5 charge (5 Lys + partially protonated N-terminus), the ''neutralization ratio'' can be calculated from the P/L (−1 charge) mixing stoichiometry. For both studied peptides, the heat release increased (in absolute value) until charge neutralization, and decreased rapidly to zero thereafter. In both cases, strong precipitation occurred when the peptides were mixed with the negatively charged DMPG at high P/L ratios, albeit more intense and faster with CA(1–8)M(1–18). Therefore, in the presence of excess peptide, an $\alpha$-helix is formed at the negative membrane, and the peptide becomes strongly attached to the lipids, destroying the membranes and inducing aggregation/precipitation, as the enthalpy decreases rapidly to zero when no more peptide is available. A similar interpretation, in the sense of ''complex formation'' between peptide and negatively charged membranes, has also been proposed by Lafleur et al. (56,57) for the interaction of melittin with DMPG, where the authors suggest that melittin tetramers bridge two adjacent bilayers, inducing membrane disruption by bilayer staking. Further, the authors also indicate that a high ionic strength (as we have in our systems) promotes self-aggregation of the peptide (58,59). Similarly, Loura et al. (60) in a FRET study also suggested that the positively charged peptides induced membrane disruption and bilayer stacking in the fluid phase, with the peptide bridging adjacent bilayers through electrostatic interaction with the anionic lipid molecules from both bilayers.

In the case of peptide titration with the mixed DMPC/DMPG (3:1) liposome system, a very interesting result was obtained. The concentration of the peptides in the cell was ~50 $\mu$M, and they were titrated with 35 mM liposome suspensions. An example of the results obtained under these conditions can be seen in Fig. 5 for the titration of CA(1–7)M(2–9) with DMPC/DMPG. As seen in the figure, there is an initial plateau value around (−0.19 ± 0.02) mJ, followed by a sigmoidal increase and another plateau at high lipid contents (the line drawn is just a ''guide for the eye'' and does not represent any curve fitting to a model). In the line of the above reasoning of ''charge neutralization'', it can be easily calculated that we are well below the neutralization ratio for most of the titration curve. It is therefore very interesting to note that the initial plateau value is the same for both peptides, a result that can be understood if we assume that at large peptide excess (as we have here at the beginning of the titration) the behavior is dominated by the attraction and partition to the negative segments of the membrane. In fact, we saw that the enthalpy was about the same for the two peptides, as they partition with helices that span about the same number of residues. Although our mixed membrane is considered to be uniform in the absence of the peptide (the two lipids DMPC and DMPG present ideal mixing), the same

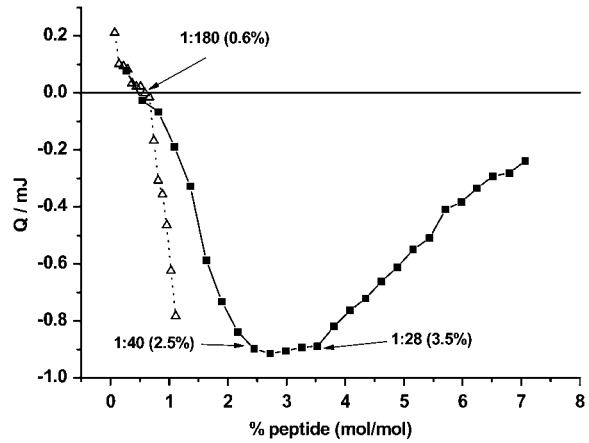


FIGURE 4 Heat per injection as a function of peptide percentage (mol/mol). (■ and *solid line*) Titration of 2.66 $\mu$L of CA(1–7)M(2–9) ($c$ = 5.38 mmol/dm$^3$) into DMPC suspension in the vessel ($c$ = 5.85 mmol/dm$^3$). (Δ and *dotted line*) Titration of 12.46 $\mu$L of CA(1–7)M(2–9) ($c$ = 2.04 mmol/dm$^3$) into DMPC suspension in the vessel ($c$ = 31.85 mmol/dm$^3$).

is not truth in its presence, as pointed out by Loura et al. (60) in their study with another peptide—the positively charged peptide induces short-range clustering of the anionic lipids. If we consider, in a simplistic approach, the ratio proposed above of 1P:5.5L (based only on charges), we can calculate the enthalpy corresponding to the plateau value of −0.19 mJ to be −44 kJ/mol$_{pep}$ for CA(1–7)M(2–9) and −49 kJ/mol$_{pep}$ for CA(1–8)M(1–18). These values are similar to the enthalpies obtained for their interaction with DMPG (−42 ± 4 and −43 ± 4 kJ/mol). The similarity suggests indeed that in this region, the behavior is dominated by the electrostatic attraction to the negative parts of the membrane surface, with $\alpha$-helix formation, in a process most similar to the interaction with purely negative membranes. It should be noted that in most cases in the literature, the plateau region is not observed, as the peptide concentrations more commonly used lead to peptide/lipid ratios that are beyond ''charge neutralization'' (51,61). But when higher peptide concentrations are used, as, e.g., in Wieprecht et al. (52), where the peptide concentration was 50 $\mu$M, the initial plateau is clearly seen. In our case, as the amount of lipid increases, the sigmoidal form of the remaining curve suggests a region of cooperative partition that must involve both the negative and zwitterionic parts, until saturation is reached at ~4% (1:25). Therefore, a treatment based on a simple partition should not be fully applicable. We interpret the raising (sigmoidal) part of the curve to reflect peptide uptake with pore formation, until the threshold value of 4% (1:25) (based on total lipid, since here we must consider the involvement of both leaflets). A binding cooperativity for CA(1–7)M(2–9) was also observed by Bhargava and Feix (32), who found it to apparently saturate at ~2%. It is reasonable to expect a higher saturation point in our case as we have more negatively charged liposomes, as mentioned above.

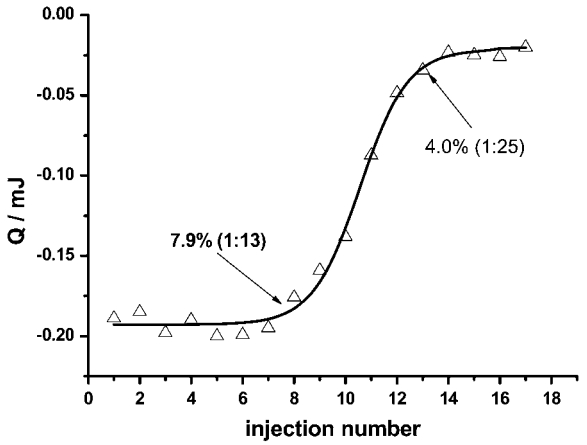


FIGURE 5 Heat per injection as a function of injection number for the titration of DMPC/DMPG (3:1) 35 mM into CA(1–7)M(2–9) (50 $\mu$M).

We should also stress that our TRFS experiments for this peptide and the membrane DMPC/DPMPG had a very marked increase in $\tau$ for low lipid content, which showed a maximum at 4% (1:25), if we transform the numbers in Fig. 2 to a total lipid content. The similarity of these behaviors and threshold concentrations is remarkable, and must indeed have a physical meaning. As regarding TRFS similar measurements, a recent article by Melo and Castanho (62) also revealed the occurrence of maxima in $\bar{\tau}$ values for peptide omiganan interacting with a negative and a partially negative lipidic system. They also suggest two $K_p$ values, one based on the initial results (low peptide) and another on the leveling-off ones, as we did here. They present a very thorough analysis of their detailed fluorescence results, and propose a saturation model, as well as further discussing the biological role of saturation. We believe that in a mixed system, the superimposition of an initial region of high $K_p$, followed by another of lower partition constant as the lipid content increases, reflects the change from a partition mainly to the negative segments of the membrane followed by partition to the zwitterionic part of the mixed membrane, with a lower partition coefficient.

As regarding the Gibbs energy, if we use the values suggested by Ladokhin and White (50) from their study of the partition of melittin to POPC membranes, we obtain a range of values for CA(1–7)M(2–9) between $-17$ and $-25$ kJ/mol (for 12 residues) and for CA(1–8)M(1–18) between $-22$ and $-32$ kJ/mol (for 10 residues, as $0.40 \times 26 = 10$). If we compare these estimates with the $\Delta G$ values in Table 2, we can see that for CA(1–7)M(2–9), the range of values represents 61–91% of the total Gibbs energy change for the DMPG system, and 67–100% for DMPC. As regarding CA(1–8)M(1–18), the range of values represents 47–69% of the total Gibbs energy change for the DMPG system, and 50–74% for DMPC and DMPC/DMPG systems. As Ladokhin and White (50) also provide a slightly different estimate for $\beta$-sheet partition ($-2.5$ kJ/mol$_{res}$), and our FTIR results indicate that CA(1–8)M(1–18) partitions as a $\beta$-sheet to the DMPC membranes (see below), we did estimate the contribution in this case, which amounts to $-25$ kJ/mol, i.e., 76% of the experimental Gibbs energy change.

The estimates based on Wieprecht et al. (51) (partition of M2a to POPC/POPG) are significantly lower ($-0.5$ kJ/mol$_{res}$). This is not surprising, as their Gibbs energy values are based on partition constants that are corrected for electrostatic effects, i.e., are describing only the hydrophobic component of the partition (61), being therefore very low for the partially negative membrane they have studied ($K = 50$ M$^{-1}$). They also studied the partition of magainin to POPC membranes and found a much higher partition constant, namely $K \approx 2 \times 10^3$ M$^{-1}$. This value will provide an estimate of $-1.6$ kJ/mol$_{res}$ for partition to POPC, a value approaching the lower limit estimate provided by Ladokhin and White (50). If we transform their $K$ value (in M$^{-1}$) to a dimensionless $K_p$ value comparable to ours (both are based on partition to the outer leaflet of the liposomes), we get the value $2.8 \times 10^3$, in excellent agreement with our value for the partition of CA(1–7)M(2–9) to DMPC (see Table 2). The values obtained for Bargava and Feix (32) for the partition of CA(1–7)M(2–9) to LUVs of POPE/POPG (8:2) and POPE/POPG/CL (68:26:6) membranes, also at high ionic strength (20 mM MOPS and 100 mM KCl, pH 7.0), and low P/L ratios, also based on the outer leaflet, are $3.5 \times 10^3$ and $1.4 \times 10^4$ M$^{-1}$. The higher value obtained for the partition to the second lipid system agrees with its higher content in anionic lipid (32). Transforming these values to values comparable to ours, we get $5.0 \times 10^3$ and $2.0 \times 10^4$. Our partition constant for this peptide to the mixed system was difficult to evaluate, but above we provided two values, one for the initial part of the TRFS titration curve (high P/L ratios) and another to the final part (lower P/L ratios), $1.0 \times 10^5$ and $1.3 \times 10^4$, respectively. Bargava and Feix (32) also observed that there was no linear response in the full concentration range, as an upward curvature was observed in the binding isotherms at relatively low mole fractions of bound peptide, suggesting a positive cooperativity in the early stages of membrane binding, exactly as we found by calorimetry and TRFS. As a result, they used only the linear parts of the plot of $X_b = f(C_f)$ for $K_p$ calculation (appearing at intermediate concentrations). Our partition constant based at the end part of our curve is of the same order of magnitude as the one they obtained for the more negative system, similar to ours in anionic lipid content ($1.3 \times 10^4$ vs. $2.0 \times 10^4$) and higher for the value based on the initial points ($1.0 \times 10^5$). Taking into account the calculation procedures and the differences in lipid type (DMPC instead of DMPE), we believe that this represents an excellent agreement.

## Real-time biospecific interaction analysis by SPR

SPR analysis did not, unfortunately, contribute significantly to a further enlightening of the peptide-lipid interaction

mechanisms under study. Nevertheless, a qualitative analysis of the obtained results shows several interesting features. Typical sensorgrams are displayed in Fig. 6 and show that specific peptide-lipid interactions do take place and are modulated by the lipid composition and the peptide, as i), responses increase along with peptide concentration (Fig. 6 *A*), and ii), sensorgrams are distinct for different peptide-lipid pairs (Fig. 6, *B–D*). The responses (in resonance units) are clearly higher for CA(1–8)M(1–18), which reflects the higher molecular weight of this peptide, as compared to its shorter analog, CA(1–7)M(2–9). The differences between peptide responses are also influenced by interaction phenomena, as Fig. 6, *B–D*, show that the difference in magnitude depends on the lipid bilayer (note the different scales). If we compare the responses for both peptides on each model membrane, we can see that on DMPG surfaces, CA(1–8)M(1–18) displays markedly higher binding responses than those of CA(1–7)M(2–9) and, further, although the effect of peptide concentration on response is significant for the first peptide, it does not affect the response in the case of the second (Fig. 6 *C*).

In the case of DMPC bilayers, responses are again higher for the longer peptide, but differences between peptides are less marked and the effect of peptide concentration is similar for both (Fig. 6 *D*). Nevertheless, for CA(1–7)M(2–9), the response reaches a plateau for the concentration 12.5 $\mu$M but not for the higher concentration of 100 $\mu$M, as opposed with what was observed with DMPG, where a plateau was reached for both concentrations with resonance units values that were independent of concentration. For CA(1–8)M(1–18), the main difference when compared to DMPG response is that the system never reaches a plateau for the higher peptide concentration. Finally, on DMPC/DMPG 3:1 surfaces, CA(1–8)M(1–18) still displays higher binding responses than CA(1–7)M(2–9) and the effect of peptide concentration is strong for both peptides, but more accentuated for the first (Fig. 6 *B*). Further, the effect of concentration for CA(1–7)M(2–9) is clearly intermediate on DMPC/DMPG 3:1 as compared to the two previous systems—a concentration effect on response is clearly observed as in DMPC, but for the concentration 100 $\mu$M, the system is much more close to a plateau, as observed with DMPG.

If we compare more in detail the observed responses when the bilayer composition changes, we can see that they are significantly higher for the DMPG surface for CA(1–8)M(1–18)—the markedly higher binding responses observed for this peptide with DMPG indicates that larger amounts are able to bind to this surface, as compared to DMPC, in the course of injection of equal peptide concentrations. For

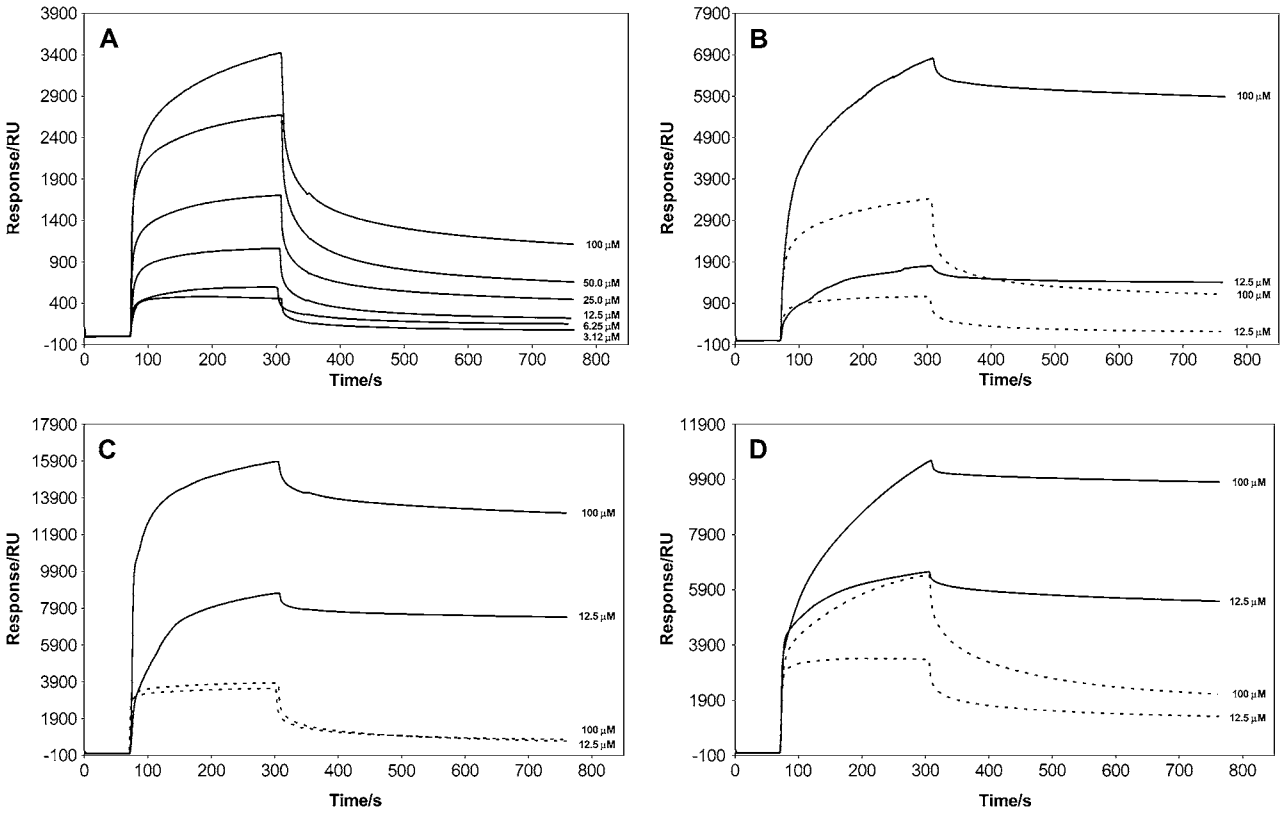


FIGURE 6 Sensorgrams for the interactions, at 35°C, of (*A*) peptide CA(1–7)M(2–9), at six different concentrations, with DMPC/DMPG (3:1); (*B*) peptides CA(1–7)M(2–9) (*dotted lines*) and CA(1–8)M(1–18) (*solid lines*) with DMPC/DMPG (3:1); (*C*) peptides CA(1–7)M(2–9) (*dotted lines*) and CA(1–8)M(1–18) (*solid lines*) with DMPG; and (*D*) peptides CA(1–7)M(2–9) (*dotted lines*) and CA(1–8)M(1–18) (*solid lines*) with DMPC.

CA(1–8)M(2–9), the effect depends strongly on concentration, whereas for the lower concentration (12.5 $\mu$M), the effect is somewhat larger on DMPG; when the concentration is 100 $\mu$M, the response is surprisingly higher with DMPC. That fact, along with what was referred to above, namely that a plateau is reached at low concentration but not at 100 mM, probably indicates that different binding modes occur above and below a given threshold concentration of CA(1–7)M(2–9).

Another relevant observation was that, in none of the experiments, was it possible to have a complete return of the response signal to the baseline level at the end of the dissociation step. The original baseline could never be recovered, even after extensive rinsing with 10 mM NaOH and 10 mM HCl (not shown), showing that either a part of the peptides remained irreversibly bound to the supported lipid bilayer or that the latter was irreversibly destroyed. This suggests that very complex phenomena were taking place, where peptide-lipid interactions cannot occur through purely electrostatic binding, as in such a case, they would be disrupted by the abrupt changes in pH imposed upon NaOH and HCl injections.

As already mentioned in Materials and Methods, all SPR analyses were run at two temperatures, 25° and 35°C. The vast majority of SPR real-time analysis of peptide-lipid interactions described in the literature were carried out at 25°C (63–67); however, this temperature is just over the $T_m$ values for DMPC and DMPG (6), so both gel and liquid crystal forms will coexist, which implies a significant degree of structural heterogeneity in the immobilized lipid surface. Therefore, we decided to run all assays at 35°C, well above the lipids' $T_m$, to ensure that the whole lipid surface was in the liquid crystalline phase, to which the peptides always display a higher partition. Notwithstanding, we have also run all assays at 25°C, for comparison with previously published data on similar systems and to ascertain whether a significant temperature dependence could be observed.

Signal stability was generally superior for experiments run at 35°C, where the curve quality was usually good even for the lowest peptide concentrations, a situation that was not verified at 25°C. The influence of temperature on binding responses depended on the injected peptide concentration (not shown). So, at low peptide concentration, sensorgrams at either temperature were virtually superimposable in both anionic and zwitterionic surfaces, whereas as peptide concentrations were increased, responses became higher at 35°C than at 25°C. This effect was more dramatic for DMPG surfaces at the highest peptide concentration assayed (100 $\mu$M).

Despite the complex interaction pattern reflected by the sensorgrams obtained, quantification of binding kinetics was attempted. Sensorgrams were generated, at both temperatures, for six different peptide concentrations (3.12–100 $\mu$M) and were tentatively analyzed by curve fitting using all reaction models available in the BIA evaluation software package. Generally, curve fitting was rather poor to any of the available models. Worse quality or inclusively nonconvergent fits were consistently obtained for all peptide-lipid pairs whenever the corresponding six sensorgrams (for the six different concentrations) were simultaneously fitted, according to the usual procedure (65,68). Convergent and better fittings, with good chi-squared values, were nevertheless achieved when each sensorgram was treated separately, but this procedure yielded unreliable rate constants, as these varied with peptide concentration. Overall, the results obtained demonstrate that peptide binding to lipids was too complex to be adequately described by standard SPR analysis, as this failed to provide reliable quantification of interaction kinetics, which can be in turn regarded as a confirmation of the above reasoning based on TSRF and isothermal titration calorimetry results.

## CONCLUDING REMARKS

Our studies show that both peptides interact with the three lipid systems. Nevertheless, significant differences were found depending on peptide and membrane system, in line with our previous findings for these systems, studied with other techniques (6). The work we presented here allowed us to get a much more complete picture of the interaction of these two hybrid peptides with model membranes, as the energetics, partition, and kinetics of the interaction, as well as peptide orientation, are addressed.

The perturbation of the lipid bilayers by a peptide is indeed governed by a balance between electrostatic and hydrophobic interactions. Our results clearly indicate the importance of electrostatics in the interaction, suggesting this effect to be highly responsible for antimicrobial activity and specificity. In fact, electrostatics is responsible for the initial attraction of the peptides to the membrane surface, leading to a much smaller bulk concentration needed for action. Further, as a consequence of opposite charge, the surface concentration at a negatively charged surface will be higher than the bulk concentration, the opposite occurring with zwitterionic membranes (model for erythrocytes). It was shown here that CA(1–7)M(2–9) can interact very effectively with DMPC membranes, but very high concentrations are needed for the interaction to lead to pore formation. This is in line with the observed antimicrobial activity—this peptide did not lyse red blood cells at concentrations $>300$ $\mu$M. On the other hand, strong evidence was provided for pore formation by this peptide in intact *Escherichia coli* cells, with an estimated pore diameter of 2.2–3.8 nm (69). The results suggest the pore to be of the toroidal type. Another study suggested also that the mechanism of action of these peptides was permeabilization of the plasma membrane of the pathogen, leading to bioenergetic collapse and cell death (25). The larger peptide was also shown to have no effect on sheep erythrocytes (24). This peptide is long enough for its helix to span the membrane, and it has been shown to require lower concentrations for activity permeabilizing the mitochondrial inner membrane, allowing the movement of both charged and noncharged solutes (26). Further, it has been shown to have strong antimicrobial activity against both Gram-positive and

Gram-negative bacteria (30,31), and has demonstrated high affinity for lipopolysaccharide, enhancing both outer and cytoplasmatic membrane permeability (29,70). We believe, in agreement with the conclusion of Ladhokin and White for melittin (36) and of Wieprecht et al. for PGLa (52), that the presence of negatively charged lipids in pathogenic agents is the key factor for specificity. Further, whereas when there are only negatively charged lipids (DMPG), the mechanism must be membrane destruction with bilayer stacking—the interaction is very strong and the helices are strongly attached to the lipids in a ''complex binding'' stoichiometry, the presence of zwitterioinic lipids in the mixed membrane brings ''plasticity'' to the interaction, and even while promoting a cooperative effect at high peptide ratios, it does not lead only to membrane destruction and precipitation, allowing a range of interaction forms to take place depending on P/L ratios. In this case, our results also suggest the formation of toroidal pores, in agreement with Pistolesi et al.'s proposal for the smaller peptide (33). CA(1–8)M(1–18) requires lower concentration for action, but its structure is less easy to control (depends significantly on preparation), and it is highly associated in buffer. Nevertheless, that might not be critical for antimicrobial activity, as we found that it could act both in $\alpha$-helix and in $\beta$-sheet forms. A very recent work showed these two peptides (CA(1–8)M(1–18) and CA(1–7)M(2–9)) to be active against colistin-resistant clinical strains (28). In that work, it was shown that the peptides show much lower minimum inhibitory concentrations than colistin and have higher affinity toward lipopolysaccharide isolated from colistin-resistant *Acinetobacter baumannii*. The authors stress that they found a strong correlation between LPS affinity and antimicrobial activity for these peptides. Again, this is in line with our proposal of a main role for electrostatics in their antimicrobial action. As regarding CA(1–8)M(1–18), our results do not allow us such strong conclusions on the preferred model for the interaction, but we would suggest that the mechanism might depend on the secondary form present, which in turn will depend on temperature, pH, and ionic strength. In any case, if we take together all our results from this work as well as from our previous study (6), we tend to think that the final step in antimicrobial action with these peptides is pore formation and not a detergent-like effect.

M.B. thanks Dr. José Catita for the access to the dynamic light scattering instrument. The authors thank Professor Ricardo Gutiérrez Gallego (Universitat Pompeu Fabra-Institut Municipal d'Investigació Mèdica, Barcelona, Spain) for the access to the SPR instrument.

P.G. thanks Conselho de Reitores das Universidades Portuguesas (Portugal) for funding through ''Acção Integrada Luso-Espanhola'' E-29/03. Thanks are also due to Fundação para a Ciência e Tecnologia for financial support to Centro de Investigação em Química (Universidade do Porto) and for a post-doctoral grant to G.B. (SFRH/BPD/5668/2001).

## REFERENCES

1. Levy, S. B. 1998. The challenge of antibiotic resistance. *Sci. Am.* 278: 46–53.
2. Zasloff, M. 2002. Antimicrobial peptides in health and disease. *N. Engl. J. Med.* 347:1199–1200.
3. Zasloff, M. 2000. Reconstructing one of nature's designs. *Trends Pharmacol. Sci.* 21:236–238.
4. Lohner, K., and E. Staudegger. 2001. Are We on the Threshold of the Post-Antibiotic Era? Horizon Scientific Press, Wymondham, Norfolk, UK.
5. Novak, R., B. Henriques, E. Charpentier, S. Normak, and E. Tuomanen. 1999. Emergence of vancomycin tolerance in *Streptococcus pneumoniae*. *Nature.* 399:590–593.
6. Abrunhosa, F., S. Faria, P. Gomes, I. Tomaz, J. C. Pessoa, D. Andreu, and M. Bastos. 2005. Interaction and lipid-induced conformation of two cecropin-melittin hybrid peptides depend on peptide and membrane composition. *J. Phys. Chem. B.* 109:17311–17319.
7. Andreu, D., and L. Rivas. 1998. Animal antimicrobial peptides: an overview. *Biopolymers.* 47:415–433.
8. Brogden, K. 2005. Antimicrobial peptides: pore formers or metabolic inhibitors in bacteria? *Nat. Rev. Microbiol.* 3:238–250.
9. Ding, J. L., and B. Ho. 2004. Antimicrobial Peptides: resistant-proof antibiotics of the new millennium. *Drug Dev. Res.* 62:317–335.
10. Hancock, R. E. W., and H. G. Sahl. 2006. Antimicrobial and host-defense peptides as new anti-infective therapeutic strategies. *Nat. Biotechnol.* 24:1551–1557.
11. Kobayashi, S., A. Chikushi, S. Tougu, Y. Imura, M. Nishida, Y. Yano, and K. Matsuzaki. 2004. Membrane translocation mechanism of the antimicrobial peptide buforin 2. *Biochemistry.* 43:15610–15616.
12. Lohner, K., and S. E. Blondelle. 2005. Molecular mechanisms of membrane perturbation by antimicrobial peptides and the use of biophysical studies in the design of novel peptide antibiotics. *Comb. Chem. High Throughput Screen.* 8:241–256.
13. Pavo, N., and Y. Shai. 2005. Host defense peptides as new weapons in cancer treatment. *Cell. Mol. Life Sci.* 62:784–790.
14. Tossi, A. 2005. Host defense peptides: roles and applications. *Curr. Protein Pept. Sci.* 6:1–3.
15. Wimley, W. C., K. Hristova, A. S. Ladokhin, L. Silvestro, P. H. Axelsen, and S. H. White. 1998. Folding of $\beta$-sheet membrane proteins: a hydrophobic hexapeptide model. *J. Mol. Biol.* 277:1091–1110.
16. van't Hof, W., E. C. I. Veerman, E. J. Helmerhosrst, and A. V. N. Amerongen. 2001. Antimicrobial peptides: properties and applicability. *Biol. Chem.* 382:597–619.
17. Veerman, E. C. I., M. Valentijn-Benz, K. Nazmi, A. L. A. Ruissen, E. Walgreen-Weterings, J. van Marle, A. B. Doust, W. van 't Hof, J. G. M. Bolscher, and A. V. N. Amerongen. 2007. Energy depletion protects *Candida albicans* against antimicrobial peptides by rigidifying its cell membrane. *J. Biol. Chem.* 282:18831–18841.
18. Hancock, R. E. W., and A. Rozek. 2002. Role of membranes in the activities of antimicrobial cationic peptides. *FEMS Microbiol. Lett.* 206:143–149.
19. Perron, G. G., M. Zasloff, and G. Bell. 2006. Experimental evolution of resistance to an antimicrobial peptide. *Proc. Biol. Sci.* 273:251–256.
20. Hancock, R. E. W., and M. G. Scott. 2000. The role of antimicrobial peptides in animal defenses. *Proc. Natl. Acad. Sci. USA.* 97:8856–8861.
21. Boman, H. G., D. Wade, A. Boman, B. Wählin, and R. B. Merrifield. 1989. Antibacterial anti-malarial properties of peptides that are cecropin-melittin hybrids. *FEBS Lett.* 259:103–106.
22. Merrifield, E. L., S. A. Mitchell, J. Ubach, H. G. Boman, D. Andreu, and R. Merrifield. 1995. D-enantiomers of 15-residue cecropin A—melittin hybrids. *Int. J. Pept. Protein Res.* 46:214–220.
23. Wade, D., D. Andreu, S. A. N. Mitchell, A. M. Silveira, A. Boman, H. G. Boman, and R. B. Merrifield. 1992. Antibacterial peptides designed as analogs or hybrids of cecropins and melittin. *Int. J. Pept. Protein Res.* 40:429–436.
24. Andreu, D., J. Ubach, A. Boman, B. Wahlin, D. Wade, R. B. Merrifield, and H. G. Boman. 1992. Shortened cecropin A-melittin

hybrids. Significant size reduction retains potent antibiotic activity. *FEBS Lett.* 296:190–194.

25. Diaz-Achirica, P., J. Ubach, A. Guinea, D. Andreu, and L. Rivas. 1998. The plasma membrane of *Leishmania donovani promastigotes* is the main target for CA(1–8)M(1–18), a synthetic cecropin A-melittin hybrid peptide. *Biochem. J.* 330(Pt. 1):453–460.
26. Diaz-Achirica, P., S. Prieto, J. Ubach, D. Andreu, E. Rial, and L. Rivas. 1994. Permeabilization of the mitochondrial inner membrane by short cecropin-A-melittin hybrid peptides. *Eur. J. Biochem.* 224:257–263.
27. Mancheño, J. M., M. Oñaderra, A. M. Del Pozo, P. Diaz-Achirica, D. Andreu, L. Rivas, and J. G. Gavilanes. 1996. Release of vesicle contents by an antimicrobial cecropin A-melittin hybrid peptide. *Biochemistry.* 35:9892–9899.
28. Saugar, J. M., M. J. Rodríguez-Hernández, B. G. de la Torre, M. E. Pachón-Ibanez, M. Fernández-Reyes, D. Andreu, J. Pachón, and L. Rivas. 2006. Activity of cecropin A-melittin hybrid peptides against colistin-resistant clinical strains of *Acinetobacter baumannii*: molecular basis for the differential mechanisms of action. *Antimicrob. Agents Chemother.* 50:1251–1256.
29. Piers, K. L., M. H. Brown, and R. E. W. Hancock. 1994. Improvement of outer membrane permeabilizing and lipopolysaccharide-binding activities of an antimicrobial cationic peptide by C-terminal modification. *Antimicrob. Agents Chemother.* 38:2311–2316.
30. Piers, K. L., and R. E. W. Hancock. 1994. The interaction of a recombinant cecropin/melittin hybrid peptide with the outer membrane of *Pseudominas aeruginosa*. *Mol. Microbiol.* 12:951–958.
31. Sawyer, J. G., N. L. Martin, and R. E. W. Hancock. 2003. Interaction of macrophage cationic proteins with the outer membrane of *Pseudomonas aeruginosa*. *Infect. Immun.* 56:693–698.
32. Bhargava, K., and J. B. Feix. 2004. Membrane binding, structure and localization of cecropin-melittin hybrid peptides: a site-directed spin-labeling study. *Biophys. J.* 86:329–336.
33. Pistolesi, S., R. Pogni, and J. B. Feix. 2007. Membrane insertion and bilayer perturbation by antimicrobial peptide CM15. *Biophys. J.* 93: 1651–1660.
34. Scott, M. G., C. M. Rosenberger, M. R. Gold, B. B. Finlay, and R. E. W. Hancock. 2000. An $\alpha$-helical cationic antimicrobial peptide selectively modulates macrophage responses to lipopolysaccharide and directly alters macrophage gene expression. *J. Immunol.* 165:3358–3365.
35. Besschiaschvili, G., and J. Seelig. 1990. Melittin binding to mixed phosphatidylglycerol/phosphatidylcholine membranes. *Biochemistry.* 29:52–58.
36. Ladokhin, A. S., and S. H. White. 2001. Detergent-like'' permeabilization of anionic lipid vesicles by melittin. *Biochim. Biophys. Acta.* 1514:253–260.
37. Bishop, C. M., W. F. Walkenhorst, and W. C. Wimley. 2001. Folding of $\beta$-sheet in membranes: specificity and promiscuity in peptide model systems. *J. Mol. Biol.* 309:975–988.
38. Chen, H. M., K. W. Leung, N. N. Thakur, A. Tan, and R. W. Jack. 2003. Distinguishing between different pathways of bilayer disruption by the related antimicrobial peptides cecropin B, B1 and B3. *Eur. J. Biochem.* 270:911–920.
39. Epand, R. M., and H. J. Vogel. 1999. Diversity of antimicrobial peptides and their mechanism of action. *Biochim. Biophys. Acta.* 1462: 11–28.
40. McClare, C. W. F. 1971. An accurate and convenient organic phosphorous assay. *Anal. Biochem.* 39:527–530.
41. Gomes, P., E. Giralt, and D. Andreu. 2001. Antigenicity modulation upon peptide cyclization: application of the GH loop of foot-and-mouth disease virus strain C1-Barcelona. *Vaccine.* 19:3459–3466.
42. Gill, S. C., and P. H. von Hippel. 1989. Calculation of protein extinction coefficients from amino acid sequence data. *Anal. Biochem.* 182: 319–326.
43. Loura, L. M. S., A. Fedorov, and M. Prieto. 1996. Resonance energy transfer in a model system of membranes: application to gel and liquid crystalline phases. *Biophys. J.* 71:1823–1836.
44. Matos, C., J. L. Lima, S. Reis, A. Lopes, and M. Bastos. 2004. Interaction of antiinflammatory drugs with EPC liposomes: calorimetric study in a broad concentration range. *Biophys. J.* 86:946–954.
45. Bastos, M., S. Hagg, P. Lonnbro, and I. Wadso. 1991. Fast titration experiments using heat conduction microcalorimeters. *J. Biochem. Biophys. Methods.* 23:255–258.
46. Cooper, M. A., A. Hansson, S. Lofas, and D. H. Williams. 2000. A vesicle capture sensor chip for kinetic analysis of interactions with membrane-bound receptors. *Anal. Biochem.* 277:196–205.
47. Hall, K., H. Mozsolits, and M.-I. Aguilar. 2003. Surface plasmon resonance analysis of antimicrobial peptide–membrane interactions: affinity and mechanism of action. *Lett. Pept. Sci.* 10:475–485.
48. March, D. 1990. Handbook of Lipid Bilayers. CRC Press, Boca Raton, FL.
49. Wimley, W. C., and S. H. White. 1996. Experimentally determined hydrophobicity scale for proteins at membrane interfaces. *Nat. Struct. Biol.* 3:842–848.
50. Ladokhin, A. S., and S. H. White. 1999. Folding of amphipathic $\alpha$-helices on membranes: energetics of helix formation by melittin. *J. Mol. Biol.* 285:1363–1369.
51. Wieprecht, T., M. Beyermann, and J. Seelig. 2002. Thermodynamics of the coil-$\alpha$-helix transition of amphipathic peptides in a membrane environment: the role of vesicle curvature. *Biophys. Chem.* 96:191–201.
52. Wieprecht, T., O. Apostolov, M. Beyermann, and J. Seelig. 2000. Membrane binding and pore formation of the antibacterial peptide PGLa: thermodynamic and mechanistic aspects. *Biochemistry.* 39:442–452.
53. Fernaández, I., J. Ubach, M. Fuxreiter, J. M. Andreu, D. Andreu, and M. Pons. 1996. Conformation and self-association of a hybrid peptide of cecropin A and melittin with improved antibiotic activity. *Chem. Eur. J.* 2:838–846.
54. Juvvadi, P., S. Vunnam, E. L. Merrifield, H. G. Boman, and R. B. Merrifield. 1996. Hydrophobic effects on antibacterial and channel-forming properties of cecropin-A-melittin hybrids. *J. Pept. Sci.* 2: 223–232.
55. Wenk, M. R., and J. Seelig. 1998. Magainin 2 amide interaction with lipid membranes: calorimetric detection of peptide binding and pore formation. *Biochemistry.* 37:3909–3916.
56. Benachir, T., and M. Lafleur. 1995. Study of vesicle leakage induced by melittin. *Biochim. Biophys. Acta.* 1235:452–460.
57. Lafleur, M., I. Samson, and M. Pézolet. 1991. Investigation of the interaction between melittin and dipalmitoylphosphatidylglycerol bilayers by vibrational spectroscopy. *Chem. Phys. Lipids.* 59:233–244.
58. Dempsey, C. E. 1990. The actions of melittin on membranes. *Biochim. Biophys. Acta.* 1031:143–161.
59. Talbot, J. C., J. Dufourcq, J. de Bony, J. F. Faucon, and C. Lussan. 1979. Conformational change and self association of monomeric melittin. *FEBS Lett.* 102:191–193.
60. Loura, L. M. S., A. Coutinho, A. Silva, A. Fedorov, and M. Prieto. 2006. Structural effects of a basic peptide on the organization of dipalmitoylphosphatidylcholine/dipalmitoylphosphatidylserine membranes: a fluorescent resonance energy transfer study. *J. Phys. Chem. B.* 110:8130–8141.
61. Wieprecht, T., M. Beyermann, and J. Seelig. 1999. Binding of antibacterial magainin peptides to electrically neutral membranes: thermodynamics and structure. *Biochemistry.* 38:10377–10387.
62. Melo, M. N., and M. A. R. B. Castanho. 2007. Omiganan interaction with bacterial membranes and cell wall models. Assigning a biological role to saturation. *BBA–Biomembranes.* 1768:1277–1290.
63. Kamimori, H., J. Blazyk, and M. I. Aguilar. 2005. Lipid membrane-binding properties of tryptophan analogues of linear amphipathic $\beta$-sheet cationic antimicrobial peptides using surface plasmon resonance. *Biol. Pharm. Bull.* 28:148–150.
64. Mozsolits, H., and M. I. Aguilar. 2002. Surface plasmon resonance spectroscopy: an emerging tool for the study of peptide-membrane interactions. *Biopolymers.* 66:3–18.

65. Papo, N., and Y. Shai. 2003. Exploring peptide membrane interaction using surface plasmon resonance: differentiation between pore formation versus membrane disruption by lytic peptides. *Biochemistry*. 42:458–466.

66. Blondelle, S. E., K. Lohner, and M. Aguilar. 1999. Lipid-induced conformation and lipid-binding properties of cytolytic and antimicrobial peptides: determination and biological specificity. *Biochim. Biophys. Acta*. 1462:89–108.

67. Papo, N., and Y. Shai. 2004. Effect of drastic sequence alteration and D-amino acid incorporation on the membrane binding behavior of lytic peptides. *Biochemistry*. 43:6393–6403.

68. Morton, T. A., D. G. Myszka, and I. M. Chaiken. 1995. Interpreting complex binding kinetics from optical biosensors: a comparison of analysis by linearization, the integrated rate equation and numerical integration. *Anal. Biochem.* 227:176–085.

69. Sato, H., and J. B. Feix. 2006. Osmoprotection of bacterial cells from toxicity caused by antimicrobial hybrid peptide CM15. *Biochemistry*. 45:9997–10007.

70. Scott, M. G., Y. Yano, and R. E. W. Hancock. 1999. Biological properties of structurally related alpha-helical cationic antimicrobial peptides. *Infect. Immun*. 67:2005–2009.